

# Constrained Black-Box Attacks Against Cooperative Multi-Agent Reinforcement Learning

Amine Andam<sup>1</sup>, Jamal Bentahar<sup>2,3</sup>, Mustapha Hedabou<sup>1</sup>

<sup>1</sup>Mohammed VI Polytechnic University

<sup>2</sup>Khalifa University

<sup>3</sup>Concordia University

amine.andam@um6p.ma, jamal.bentahar@ku.ac.ae, mustapha.hedabou@um6p.ma

## Abstract

Collaborative multi-agent reinforcement learning has rapidly evolved, offering state-of-the-art algorithms for real-world applications, including sensitive domains. However, a key challenge to its widespread adoption is the lack of a thorough investigation into its vulnerabilities to adversarial attacks. Existing work predominantly focuses on training-time attacks or unrealistic scenarios, such as access to policy weights or the ability to train surrogate policies. In this paper, we investigate new vulnerabilities under more challenging and constrained conditions, assuming an adversary can only collect and perturb the observations of deployed agents. We also consider scenarios where the adversary has no access at all (no observations, actions, or weights). Our main approach is to generate perturbations that intentionally misalign how victim agents see their environment. Our approach is empirically validated on three benchmarks and 22 environments, demonstrating its effectiveness across diverse algorithms and environments. Furthermore, we show that our algorithm is sample-efficient, requiring only 1,000 samples compared to the millions needed by previous methods.

## 1 Introduction

Collaborative multi-agent reinforcement learning (c-MARL) algorithms have demonstrated state-of-the-art performances in complex cooperative tasks [Rashid *et al.*, 2018; Yu *et al.*, 2022], making them well-suited for solving real-world problems across various domains [Lv *et al.*, 2025; Park *et al.*, 2024; Zhang *et al.*, 2024]. However, a critical prerequisite for the widespread adoption of c-MARL is a full understanding of its vulnerabilities to adversarial attacks [Huang *et al.*, 2017; Kos and Song, 2017], particularly when deployed.

While much of the literature on adversarial c-MARL focuses on training-time attacks [Zheng *et al.*, 2023; Liu and Lai, 2023; Chen *et al.*, 2024; Hu and Zhang, 2022], we focus instead on test-time attacks, where the adversary is present during deployment. Prior work on test-time attacks [Pham *et al.*, 2023; Lin *et al.*, 2020; Nisioti *et al.*, 2021] has primarily considered white-box threat models, in which the adversary

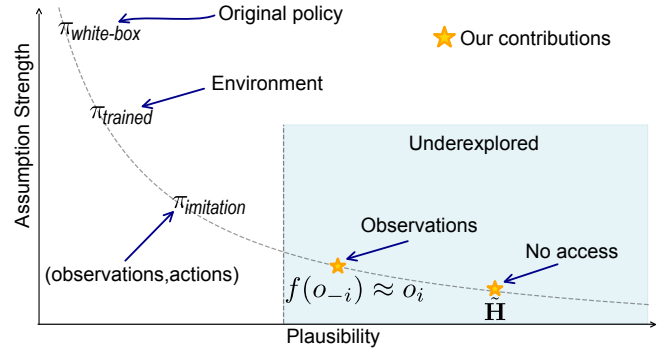


Figure 1: Assumption Strength vs Plausibility.

has access to the policy architecture and weights. This scenario is not always feasible. Moreover, such access can itself be considered a successful attack, as it typically involves proprietary knowledge with significant financial implications if leaked. In contrast, black-box threat models [Huang *et al.*, 2017] do not assume access to the policy's weights or architecture; instead, they often involve learning a surrogate policy network either by training from scratch in the same environment [Huang *et al.*, 2017] or through imitation learning [Wu *et al.*, 2021; Inkawich *et al.*, 2020]. The former requires access to the training environment, while the latter relies on collecting both observations and actions or the ability to query the model (see Figure 1). But what if the adversary cannot access such information to train a surrogate policy?

In our work, we examine test-time attacks against c-MARL in black-box settings, but we push the standard assumptions a step further: we consider an adversary whose access is restricted to the observations (no access to the actions) of deployed agents, referred to as infected agents. The adversary does not have full control over these infected agents; instead, they can only add small perturbations to their observations.

**Our first main contribution** is to show that such an adversary can effectively sabotage a c-MARL system, causing significant damage with as few as 1,000 collected samples, compared to the millions required by previous methods [Pham *et al.*, 2023]. Our idea is to generate small perturbations that cause agents to have inconsistent views of the same environment; we refer to this as misalignment. For instance, in a Pursuit game [Gupta *et al.*, 2017], where two agents must co-

Table 1: Comparison with prior work.

Paper	Test-time	Black-box	Accessible Elements					Target			
			Policy	Obs	Actions	Reward	Env	Actions	Obs	Reward	Env
Pham et al. (2023) [Pham <i>et al.</i> , 2023]	✓	✗	✓	✓	✓	✓	✓	✗	✓	✗	✗
Lin et al. (2020) [Lin <i>et al.</i> , 2020]	✓	✗	✓	✓	✓	✓	✓	✗	✓	✗	✗
Nisioti et al. (2021) [Nisioti <i>et al.</i> , 2021]	✓	✗	✓	✓	✓	✓	✗	✓	✗	✗	✗
Chen et al. [Chen <i>et al.</i> , 2025]	✓	✓	✗	✓	✓	✓	✓	✗	✓	✗	✗
Hu and Zhang (2022) [Hu and Zhang, 2022]	✗	✗	✓	✓	✓	✓	✓	✓	✗	✗	✗
Chen et al. (2024) [Chen <i>et al.</i> , 2024]	✗	✗	✓	✓	✓	✓	✓	✓	✗	✗	✗
Liu and Lai (2023) citeliu2023efficient	✗	✓	✗	✓	✓	✓	✓	✓	✗	✓	✗
Zheng et al. (2023) [Zheng <i>et al.</i> , 2023]	✗	✓	✗	✓	✓	✓	✗	✗	✓	✗	✗
<b>Ours</b>	✓	✓	✗	(✓,✗)	✗	✗	✗	✗	✓	✗	✗

operate to surround a moving target, if an adversary causes each agent to observe a different target position, their ability to coordinate is severely compromised. We design our perturbations to induce this effect and refer to the resulting attack as the **Align attack**.

**Our second main contribution** introduces an even more constrained attack. We consider an adversary with no access whatsoever (no observations, actions, or weights), having only the ability to perturb each agent’s observation. The literature refers to this setting as free attacks, which predominantly rely on random noise injection. In contrast, we apply the same misalignment principle and propose a novel attack using partial Hadamard matrices to generate structured perturbations. As discussed in Section 4.5, misalignment can be induced through orthogonal matrices. We refer to this attack as the **Hadamard attack**.

Moreover, we propose a targeted attack that combines ideas from both methods by using observations to identify critical agents and Hadamard matrices to craft adversarial perturbations. This leverages the profiling capability of the Align attack and the fast generation of the Hadamard attack, resulting in an efficient and lightweight attack.

Our contributions are illustrated in Figure 1. Most prior work considers attacks that require access to some form of policy, real or surrogate, and tend to be effective. However, such methods rely on strong access assumptions, which limit their plausibility. In contrast, we study threat models with weak access, which are more challenging and remain underexplored. In general, fewer attacker assumptions lead to more plausible attacks. Figure 1 illustrates this inverse relationship between attack plausibility and threat model strength.

Finally, we conduct extensive experiments on three MARL benchmarks and 22 tasks, covering fully observable, partially observable, and highly cooperative settings, along with appropriate ablation studies.

## 2 Related works

Adversarial c-MARL can be classified according to several criteria: Does the attack occur during training or deployment? Are we considering a white-box or black-box scenario? What system components does the attacker have access to, and which does it target?

**Training-time vs Test-time attacks.** Training-time attacks, also called data poisoning attacks [Rakhsha *et al.*, 2020], occur when an adversary is present during the training and aim

to manipulate the agent into a target policy. This can involve reward poisoning [Liu and Lai, 2023; Zhang *et al.*, 2020], environment poisoning [Rakhsha *et al.*, 2021], or altering observations or actions [Hu and Zhang, 2022; Chen *et al.*, 2024; Zheng *et al.*, 2023]. However, interfering with training is not always feasible. MARL systems are arguably more vulnerable when deployed. Test-time attacks occur during deployment and aim to degrade agent performance. This is achieved by exploiting the known vulnerabilities of neural networks to adversarial inputs [Huang *et al.*, 2017; Szegedy, 2013], mainly through observation manipulation [Pham *et al.*, 2023; Lin *et al.*, 2020], or action manipulation [Nisioti *et al.*, 2021].

**White-box vs Black-box.** In white-box scenarios, the attacker knows the learning algorithm and has access to the policy weights and its architecture [Chen *et al.*, 2024; Hu and Zhang, 2022; Nisioti *et al.*, 2021; Lin *et al.*, 2020; Pham *et al.*, 2023; Huang *et al.*, 2017]. While these attacks tend to be the most effective, it is impractical for the attacker to have the complete knowledge of the deployed policies. Conversely, black box settings allow for more relaxed assumptions [Huang *et al.*, 2017]. Most existing work relies on learning a surrogate policy to exploit the transferability of adversarial examples [Papernot *et al.*, 2016]. This surrogate policy can be learned by training the model from scratch [Huang *et al.*, 2017], but doing so requires access to the training environment. Alternatively, imitation learning can be used to approximate the policy [Wu *et al.*, 2021; Inkawich *et al.*, 2020], which would necessitate access to observation-action pairs or the ability to query the policy.

Table 1 provides a comprehensive comparison between our work and previous work. Prior work on test-time attacks often assumes white-box adversaries and access to multiple elements simultaneously, which is not always feasible during deployment. We instead focus on more practical scenarios: deployed c-MARL in a black-box setting with limited access.

## 3 Background

Consider a neural network  $f$  parameterized by  $\theta$ , which takes an input  $x \in \mathcal{X}$  and outputs  $y$ , and is trained to minimize a loss function  $J$ . An adversarial attack aims to add a perturbation  $\delta$  to the input  $x$  that maximizes the loss  $J(x + \delta, y; \theta)$ . Moreover,  $\delta$  must remain small to avoid detection, which is enforced by constraining its  $L_\infty$  norm with a budget  $\epsilon$ . This problem is formulated as:

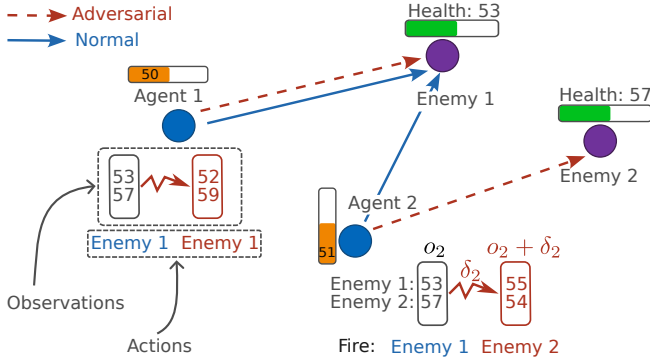


Figure 2: Coordination is prevented by flipping the lowest-health enemy as seen by each agent.

$$\delta = \arg \max_{\delta} J(x + \delta, y; \theta) \quad \text{subject to} \quad \|\delta\|_{\infty} \leq \epsilon \quad (1)$$

Many methods have been proposed to find  $\delta$ . Fast Gradient Signed Methods (FGSM) [Goodfellow *et al.*, 2014] is a simple technique that computes the perturbations as:

$$\delta = \epsilon \times \text{sign}(\nabla_x (J(x, y; \theta))) \quad (2)$$

where  $\nabla_x (J(x, y; \theta))$  is the gradient of the loss function  $J$  with respect to the input  $x$  and  $\text{sign}$  is a function which returns  $+1$  if the argument is positive,  $-1$  if negative, and  $0$  if zero.

FGSM is a single-step attack. A stronger multistep variant is Projected Gradient Descent (PGD) [Kurakin *et al.*, 2018; Madry *et al.*, 2018] which applies iterative perturbations over  $K$  steps with a small step size  $\alpha$ . After each step, the perturbed input is projected back into the valid domain  $\mathcal{X}$ :

$$x_0^* = x, x_{t+1}^* = \text{Clip}_{\mathcal{X}}\{x_t^* + \alpha \times \text{sign}(\nabla_x J(x_t^*, y; \theta))\} \quad (3)$$

where  $\text{Clip}_{\mathcal{X}}$  is an element-wise clipping operator that ensures the results remain within the valid domain  $\mathcal{X}$ .

Using FGSM or PGD against a c-MARL system requires access to the agents' policy or value networks in order to compute the loss in Equation 1. Since we consider attacks in a black-box setting, the main challenge our paper tries to solve is how to circumvent the need for direct access to the policy and still be able to use powerful methods like PGD.

## 4 Methodology

### 4.1 Problem statement

We consider a cooperative multi-agent system during its deployment phase. Let  $\mathcal{N} = \{1, \dots, n\}$  be the set of agents. We denote by  $o_i$  the observation of agent  $i$ , which is of dimension  $d$ ,  $o_{-i}$  is the concatenated observations of all the agents except agent  $i$ , and  $\mathbf{o}$  is the joint observation. The adversary cannot directly control the agents' actions but can inject small perturbations into their observations before the policy networks process them. This assumption is standard in adversarial c-MARL (see Section 2).

### 4.2 Intuition

In cooperative tasks, effective collaboration depends on agents having aligned perceptions and beliefs about their environment. By aligned perceptions, we mean that agents observing the same object receive consistent information about its attributes. For instance, in the SMAC benchmark [Ellis *et al.*, 2024], agents cooperate to defeat enemy units, which requires skills such as *focus fire*, where agents jointly attack a single opponent to eliminate it quickly. This typically involves selecting the weakest enemy based on health level. Effective coordination therefore requires agreement on the target's health and position. Adversarial manipulation of these perceptions, as shown in Figure 2, can disrupt coordination.

We do not necessarily assume that the agents must observe the same objects. The same intuition applies to partially observable environments where there is minimal to no overlap between agents' observations. In this case, our goal is to induce misalignment in the common beliefs among the agents [Zhang *et al.*, 2022; Moreno *et al.*, 2021]. Accordingly, our experiments mainly focus on partially observable tasks.

Overall, our attack exploits agents' dependence on aligned perceptions by manipulating their observations. Our idea is similar to a divide-and-conquer strategy: we make each agent perceive the environment differently, which undermines coordination and ultimately degrades team performance.

### 4.3 The Align attack

Cooperative MARL typically assumes that agents have aligned perceptions. Under this assumption, agents' observations  $\{o_1, \dots, o_n\}$  are initially aligned. Our goal is to perturb each observation so that the modified observations  $\{o_1 + \delta_1, \dots, o_n + \delta_n\}$  become misaligned. Therefore, we first need a quantitative measure of misalignment.

Aligned observations are correlated because they encode similar information and beliefs about the environment. As a result, one agent's observation  $o_i$  can be approximated from the observations of other agents  $o_{-i}$ . In contrast, misaligned observations exhibit weaker correlation, making such an approximation difficult.

Formally, aligned observations allow us to train the following neural network  $f_{\theta}$  using the mean squared error  $J(\mathbf{o}; \theta)$ :

$$f_{\theta}(o_{-i}) \approx o_i \quad \forall i \in \mathcal{N} \quad (4)$$

$$J(\mathbf{o}; \theta) = \frac{1}{n} \sum_{i \in \mathcal{N}} (f_{\theta}(o_{-i}) - o_i)^2 \quad (5)$$

Once  $f_{\theta}$  is properly trained, it can be used to measure misalignment, as high loss values are associated with misaligned observations. Therefore, our strategy to induce misalignment is to find small perturbations  $\{\delta_i\}_{i \in \mathcal{N}}$  that will maximize the loss of the trained network  $f_{\theta}$ . This is formally expressed as:

$$\delta = \arg \max_{\delta} J(\mathbf{o} + \delta; \theta) \quad \text{s.t.} \quad \|\delta\|_{\infty} \leq \epsilon \quad (6)$$

The main benefits of our formulation in Equation (6) are threefold. First, it is black-box and does not require access to policy parameters. Second, unlike prior attacks, it does not rely on any policy or value function to generate perturbations. Third, it enables the use of PGD attacks similar to those

in Equation (1). However, a subtle but important distinction must be noted. In Equation (1), the perturbation is added only to the input, whereas in Equation (6), it is added to both the input and the output.

To summarize, our attack consists of two phases. In the first phase, we collect the observations of deployed agents for a sufficient period  $\mathcal{T}^c$ , which are then used to train  $f_\theta$ . No attack is executed during this phase. In the second phase, we intercept the current observations  $\{o_i\}_{1,\dots,n}$ , generate the corresponding perturbations, and inject them into the agents. A full and detailed pseudocode can be found in the appendix.

#### 4.4 Targeted Align attack

Attacking all agents may be computationally expensive and may reduce the stealthiness of the attack. Therefore, we may be forced to only attack a subset of agents  $\mathcal{M} \subset \mathcal{N}$  with  $m = |\mathcal{M}| < n$ . For a targeted attack, we choose the subset of agents whose observations are most mutually aligned; we interpret them as agents who are most likely to coordinate among each other, and we aim to undermine their collaboration. Formally, for a fixed number of targeted agents  $m$ , we seek the subset  $\mathcal{M}$  that satisfies the following:

$$\mathcal{M} = \arg \min_{\substack{\mathcal{S} \subset \mathcal{N} \\ |\mathcal{S}|=m}} J(\{o_i\}_{i \in \mathcal{S}}; \theta) = \sum_{i \in \mathcal{S}} (f_\theta(o_{-i}) - o_i)^2 \quad (7)$$

#### 4.5 Free misalignment attacks

Our goal is to exploit alignment without access to observations. To illustrate our method, imagine a two-dimensional game in which two agents must jointly catch an object. Each agent observes the  $(x, y)$  coordinates of the target. An adversary can manipulate their observations by pushing them toward completely different directions to prevent them from jointly catching the target. A suitable strategy is to push the agents in perpendicular directions<sup>1</sup>. This idea generalizes to high-dimensional observations using **vector orthogonality**.

To design a misalignment attack, we will generate a matrix  $\delta = [\delta_1^\top \dots \delta_n^\top] \in \mathbb{R}^{n \times d}$  that must satisfy two conditions:

1. *Condition 1:* The rows are orthogonal :

$$\delta_i^\top \delta_j = 0 \quad \forall i, j \in \mathcal{N}, i \neq j, \quad (8)$$

2. *Condition 2:* Satisfy the attack budget constraint

$$\|\delta_i\|_\infty \leq \epsilon \quad \forall i \in \mathcal{N} \quad (9)$$

Generating such perturbations is nontrivial. Greedy construction can satisfy the budget constraint but often fails to ensure orthogonality, especially in high dimensions. Sampling and orthogonalizing a random matrix guarantees orthogonality but not the budget constraint (low magnitudes).

To generate perturbations that satisfy both constraints, we use **partial Hadamard matrices**  $\tilde{\mathbf{H}}$  which are obtained by selecting a subset of rows from a full Hadamard matrix  $\mathbf{H}$ .

<sup>1</sup>We did not choose opposite directions as we cannot generalize the idea with more than 2 agents. We cannot have a set of three or more vectors where every pair points into opposite directions.

Hadamard matrices have orthogonal rows, whose entries are either  $+1$  or  $-1$ . Thus, it is clear that the following matrix satisfies both conditions (1) and (2):

$$\delta = \epsilon \times \tilde{\mathbf{H}} \quad (10)$$

Hadamard matrices exist only for specific dimensions: when  $d$  is a multiple of 4. To bypass this, we generate a full Hadamard matrix of size  $\tilde{d}$ , where  $\tilde{d}$  is the largest power of two such that  $\tilde{d} \leq d$ :

$$\tilde{d} = 2^{\lfloor \log_2 d \rfloor} \quad (11)$$

We then pad the remaining columns with zeros. This padding affects neither orthogonality nor the budget constraint. We use *Sylvester's construction* to generate Hadamard matrices.

## 5 Experiments

The goal of this section is to thoroughly investigate the performance of our attacks. To this end, we deliberately select multiple environments from three different MARL benchmarks, each chosen with a specific purpose to evaluate distinct aspects of our approach.

- Level-Based Foraging (LBF) [Papoudakis *et al.*, 2021]: is a grid-world environment where agents collect scattered food. We select fully observable, highly cooperative, and partially observable tasks. In fully observable tasks, agents observe the entire grid. In the highly cooperative setting (“-coop” in Figure 5), food is collected only if all agents surround it simultaneously, leading to overlapping observations that facilitate training  $f_\theta$ . Partially observable tasks are more challenging: agents see only a limited area around them (2-square or 1-square radius, with “-2s” or “-1s” flags). We use 10 LBF environments, with observation dimensions ranging from 15 to 18. The maximum number of agents is 4.
- Multi-Robot Warehouse (RWARE) [Papoudakis *et al.*, 2021]: is a partially observable multi-agent environment where robots are tasked with collecting requested shelves inside a warehouse. We test with three different levels of partial observability, where agents observe a  $7 \times 7$ ,  $5 \times 5$ , or  $3 \times 3$  grid around them (“sr-3”, “sr-2” and “sr-1” flags in Figure 4). In addition to partial observability, this benchmark allows experiments with higher-dimensional observations, ranging from 71 to 351. The number of agents is 4 in all the tasks.
- StarCraft Multi-Agent Challenge (SMAC) [Ellis *et al.*, 2024]: SMAC is the most used benchmark in c-MARL and provides partially observable environments with a large number of agents, allowing us to evaluate how our algorithms scale. Since SMAC tasks are combat scenarios, agents can be removed during an episode due to death, leading to situations where the adversary loses access to some agents. This setting allows us to evaluate the robustness of our attacks under partial and dynamic access, where not all agents can be attacked throughout the episode. Such conditions reflect many realistic scenarios in which adversarial capabilities may be limited

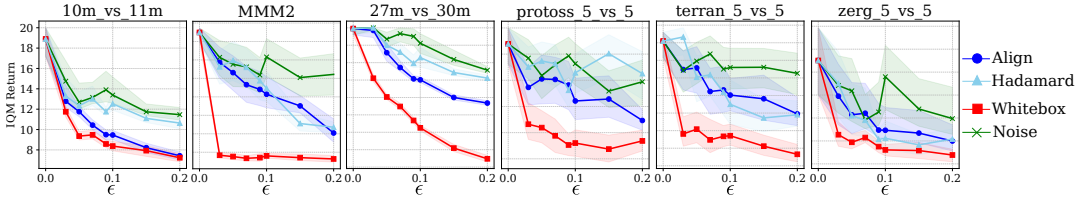


Figure 3: Performance on SMAC: IQM returns and 95% CIs estimated using 50 runs.

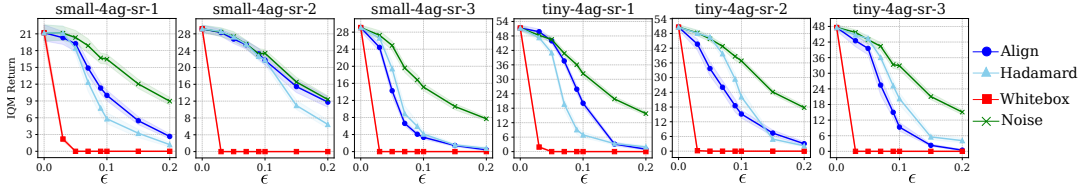


Figure 4: Performance on RWARE: IQM returns and 95% CIs estimated using 50 runs.

or intermittent. We selected six games with observation dimensions ranging from 82 to 285, and with 5, 10, or 27 agents.

**Adversarial baselines:** We use the following baselines: (1) White-box attack. (2) Random attacks. Most previous works considered only uniform and normal distributions. In addition, we include a non-symmetric distribution (exponential  $\text{Exp}(\lambda)$ ) and temporally correlated noise generated using the Ornstein–Uhlenbeck (OU) process. We report the performance of the best random attack (i.e, the random noise with the lowest return). Although comparing our limited-access attacks to a white-box attack is not entirely fair, we include it to estimate an upper bound and to select meaningful values for the attack budget as it is pointless to choose  $\epsilon$  where the random attacks outperform the white-box attack.

As we consider test-time attacks, we train the agents in each environment using QMIX [Rashid *et al.*, 2018] and MAPPO [Yu *et al.*, 2022]. We test different architectures to train  $f_\theta$ : feedforward, recurrent, and the encoder-only transformer. Unless otherwise stated, the results in the subsequent paragraphs are of agents trained with MAPPO, and the adversary collects a dataset of observations from 5,000 environment transitions and uses RNNS to train  $f_\theta$ . We fix PGD iterations at  $K = 10$  and the step size of  $\alpha = \frac{\epsilon}{K}$ . Full details of the used hyperparameters and additional results can be found in the appendix.

**Metrics:** We evaluate our attacks using episodic return. To ensure robust results, we report the interquartile mean (IQM) [Agarwal *et al.*, 2021] of returns over 50 independent episodes, along with 95% confidence intervals. IQM is robust to outliers and less biased than the median. Our code is open-source.<sup>2</sup>

## 5.1 Numerical results

Figures 3, 4, and 5 present the IQM returns (y-axis) for SMAC, RWARE, and LBF benchmarks, respectively, across

selected  $\epsilon$  values (x-axis). The values at  $\epsilon = 0$  represent the benign performance of the agents during deployment.

- **LBF** (Figure 5): We observe that both Align and Hadamard attacks are effective in both fully and partially observable tasks (first two vs last three columns). Comparing each task with its highly cooperative variant (1st vs 2nd, and 3rd vs 4th columns), attacks are substantially more effective in highly cooperative settings, leading to much lower returns. Notably, in most partially observable scenarios, the Hadamard attack, despite being a free attack, matches or even outperforms the Align attack. The same pattern is observed on the RWARE benchmark.

- **RWARE** (Figure 4): Overall, both attacks are effective across tasks. Under the strongest partial observability (sr = 1, 1st and 4th columns), the Align attack remains effective but is outperformed by Hadamard. As partial observability decreases (e.g, from the 1st to the 3rd column), the performance gap narrows, as learning a good network  $f_\theta$  becomes easier. Results on RWARE further indicate that attack effectiveness is not degraded by high dimensional observations.

- **SMAC** (Figure 3): The Align attack exhibits consistent performance across all games. In contrast, the Hadamard attack struggles to achieve significant gains over random noise in several scenarios (1st, 3rd, and 4th columns). Beyond partial observability and high dimensionality, SMAC further demonstrates that the Align attack remains effective in scenarios with large numbers of agents and without persistent access to the agents.

Next, we evaluate targeted attacks. For a fixed number of agents  $m$ , the Align attack uses the targeted procedure from Section 4.4, while Hadamard selects agents randomly. Results are shown in Figures 6, 7, and 8, with the number of attacked agents indicated at the right of each subplot. Two observations stand out: first, Align maintains strong performance when 50% or more agents are targeted; second, Align is less sensitive than Hadamard to targeting fewer agents. To illustrate this second point, in Figures 7 and 8 we specifically show tasks where Hadamard outperforms Align when all agents are attacked, but as fewer agents are targeted, Align

<sup>2</sup>Github: <https://github.com/AmineAndam04/black-box-marl.git>

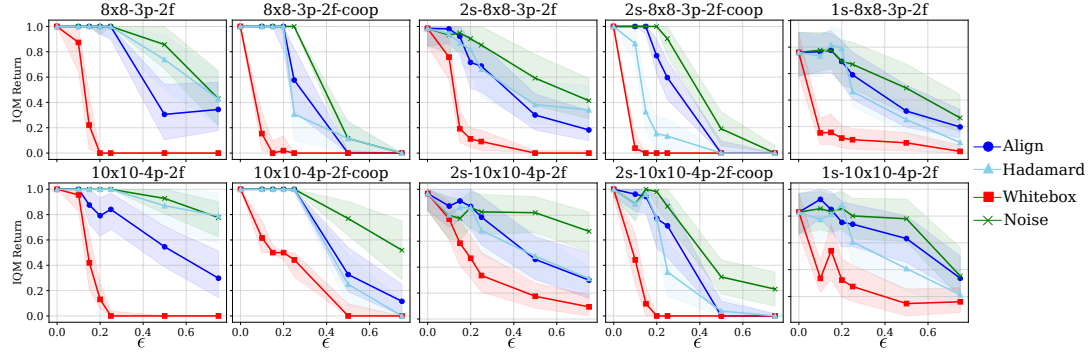


Figure 5: Performance on LBF: IQM returns and 95% CIs estimated using 50 runs.

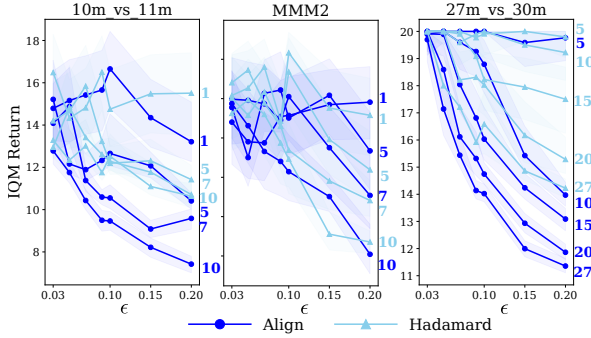


Figure 6: Performance of targeted attacks on SMAC.

becomes more effective.

The last remark also indicates that the Align attack effectively identifies vulnerable agents. To further test this, we isolate the targeting mechanism: we select agents using the Align network (Equation 7) but inject Hadamard perturbations instead of Align perturbations.

In Tables 2 and 3, we report the performance gap between Hadamard attack obtained with and without selection mechanisms. For example, if the untargeted Hadamard attack causes a -15% drop relative to the benign return and the table reports a -10% drop, this means that the targeted Hadamard attack yields a total drop of -25%. Across all benchmarks, the targeted Hadamard attack consistently outperforms the untargeted variant, with a performance gap of more than two digits in many environments, with a maximum additional drop of -57%. On average across all the tasks, the additional drop is -11.5% on LBF, -6.18% on RWARE, and -6.28% on SMAC. These results demonstrate the effectiveness of the alignment network  $f_\theta$  for target selection.

## 5.2 Ablations

To normalize returns across tasks with different magnitudes, the y-axis in the following figures reports the percentage drop in return caused by our attack relative to the benign reward.

**Data collection:** Figure 9 evaluates the Align attack with training data ranging from 1,000 to 100,000 steps. Surprisingly, a strong attack performance is achieved with few samples, with no observable gains from larger datasets. This reduces data collection requirements, which improves the

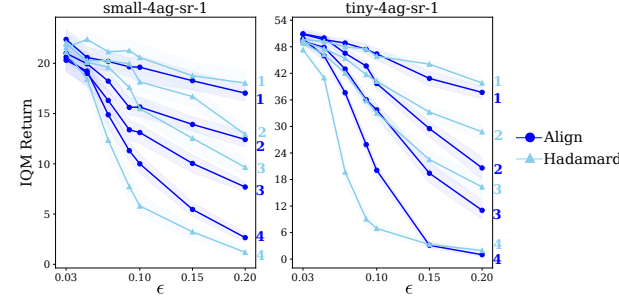


Figure 7: Performance of targeted attacks on RWARE.

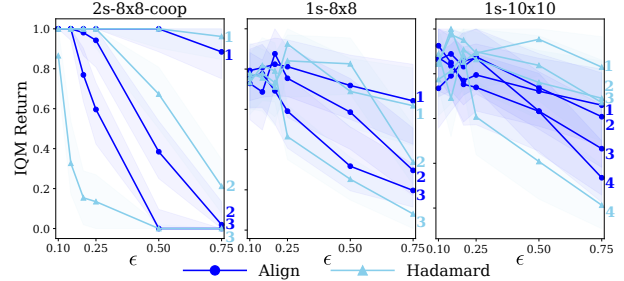


Figure 8: Performance of targeted attacks on LBF.

stealth of the attack and lowers storage and training costs for the adversary.

**Network architecture:** Figure 10 compares the Align attack across different neural architectures. Across all benchmarks, RNNs generally achieve the strongest performance, with a particularly large margin on RWARE. MLPs and Transformers perform comparably, but MLPs provide a better cost-performance trade-off due to faster training with only three hidden layers. RNNs share this advantage, as we employ shallow variants with one or two recurrent layers. We also tested deeper and more complex architectures, but they did not yield further performance gains.

**PGD and FGSM:** We investigate the impact of the number of PGD steps  $K$ . Figure 11 compares performance for  $K \in \{1, 5, 10\}$ . A key observation is that a single step is often sufficient to achieve strong performance, which is important for real-time attacks, as it allows perturbations to be generated quickly with minimal computational cost.

Task	$m$	$\epsilon = 0.15$	$\epsilon = 0.2$	$\epsilon = 0.25$
1s-10x10	2	-23.57	-4.99	-6.6
	3	2.32	-6.28	-7.48
1s-8x8	1	-6.01	-0.96	-19.24
	2	-7.42	-0.79	-19.34
2s-8x8-coop	1	0	-3.84	-3.84
	2	-32.69	-48.07	-57.69

Table 2: Targeted Hadamard attack on LBF

Task	$m$	$\epsilon = 0.05$	$\epsilon = 0.09$	$\epsilon = 0.15$
tiny-4ag-sr-1	1	0.22	-0.37	-4.50
	3	-1.35	-2.1	-16.80
small-4ag-sr-1	1	-9.80	-6.71	-2.35
	3	-2.17	-14.51	-19.23
10m_vs_11m	3	-8.3	-10.17	-3.71
	7	-14.35	0.40	1.98
MMM2	3	3.26	0.73	-6.32
	7	-2.76	1.22	-7.10

Table 3: Targeted Hadamard attack on RWARE and SMAC

### 5.3 Discussion

Most adversarial MARL work, including ours, evaluates attack effectiveness primarily using episodic return. We believe episode length is another important metric that is often overlooked, particularly in real-world scenarios with constrained adversaries. In such settings, fully incapacitating the c-MARL system is not always realistic; a more plausible outcome is delaying task completion by increasing episode length, even if tasks are eventually completed. Longer episodes can substantially increase operational costs, including energy and computation, making this a meaningful measure of adversarial impact. We illustrate this using the Align attack on LBF. Table 4 shows percentage increases in episode length, which often exceed double digits and reach up to 226% in the worst case.

Tasks	$\epsilon = 0.1$	$0.15$	$0.2$	$0.25$	0.5
2s-8x8-coop	9.59	43.55	138.52	152.49	170.86
2s-10x10-coop	34.44	23.78	65.78	68.52	79.04
8x8-coop	10.59	29.67	103.86	188.56	226.80
8x8	5.94	21.06	51.93	75.93	193.21

Table 4: Episode length increase (%) on LBF tasks

**Limitations:** Our proposed algorithm faces the same core challenges as any MARL training procedure, such as partial observability, which we discuss thoroughly in the paper. In addition, issues like handling heterogeneous agents and multi-modal observations may further affect the effectiveness of our attack. Moreover, we studied realistic attacks from the perspective of the adversary’s access and capabilities. However, other perspectives can also be considered, in-

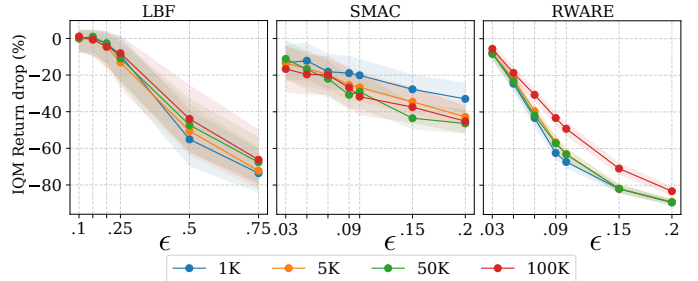


Figure 9: Collected data size effect across MARL benchmarks

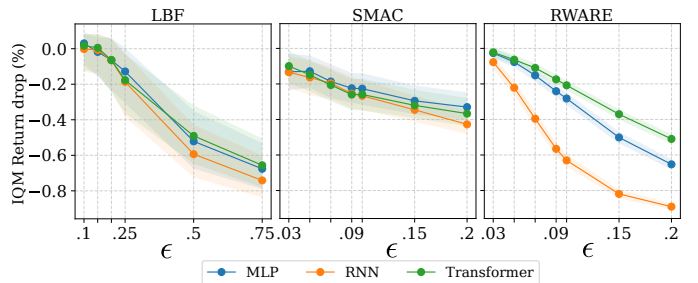


Figure 10: Neural architecture effect across MARL benchmarks

cluding system-level constraints, attack deployment, and detectability in real-world settings. We plan to address these aspects in future work.

## 6 Conclusion

In this paper, we present two novel adversarial attacks specifically designed for collaborative MARL during deployment. We consider a black-box scenario under highly constrained conditions: First, a scenario where the adversary has access solely to the observations of deployed agents. Second, a more constrained scenario where the adversary has no access at all. Our approach exploits the reliance of collaborative agents on aligned perceptions for effective cooperation and adds small perturbations to the agents’ observations specifically designed to induce misaligned perceptions. Our empirical investigation showed the effectiveness of our attacks.

Notably, our method requires minimal data to generate effective perturbations; we found that as few as 1,000 steps are sufficient to create impactful damage. Moreover, the adversary can choose to execute the attack in fewer steps while still

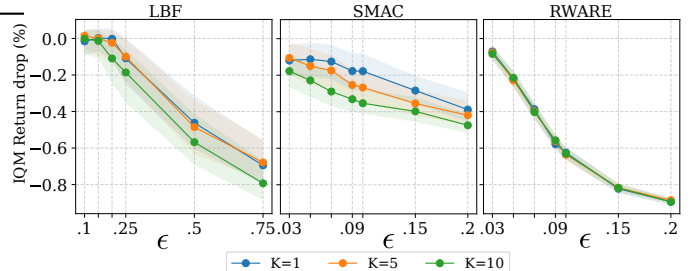


Figure 11: PGD’s iteration effect across MARL benchmarks.

achieving satisfactory results.

## References

[Agarwal *et al.*, 2021] Rishabh Agarwal, Max Schwarzer, Pablo Samuel Castro, Aaron C. Courville, and Marc G. Bellemare. Deep reinforcement learning at the edge of the statistical precipice. In Marc’Aurelio Ranzato, Alina Beygelzimer, Yann N. Dauphin, Percy Liang, and Jennifer Wortman Vaughan, editors, *Advances in Neural Information Processing Systems 34: Annual Conference on Neural Information Processing Systems 2021, NeurIPS 2021, December 6-14, 2021, virtual*, pages 29304–29320, 2021.

[Chen *et al.*, 2024] Zhen Chen, Yong Liao, Youpeng Zhao, Zipeng Dai, and Jian Zhao. Cuda2: An approach for incorporating traitor agents into cooperative multi-agent systems. *arXiv preprint arXiv:2406.17425*, 2024.

[Chen *et al.*, 2025] Jianming Chen, Yawen Wang, Junjie Wang, Xiaofei Xie, Yuanzhe Hu, Qing Wang, and Fanjiang Xu. Adversarial attack on black-box multi-agent by adaptive perturbation. *CoRR*, abs/2511.15292, 2025.

[Ellis *et al.*, 2024] Benjamin Ellis, Jonathan Cook, Skander Moalla, Mikayel Samvelyan, Mingfei Sun, Anuj Mahajan, Jakob Foerster, and Shimon Whiteson. Smacv2: An improved benchmark for cooperative multi-agent reinforcement learning. *Advances in Neural Information Processing Systems*, 36, 2024.

[Goodfellow *et al.*, 2014] Ian J Goodfellow, Jonathon Shlens, and Christian Szegedy. Explaining and harnessing adversarial examples. *arXiv preprint arXiv:1412.6572*, 2014.

[Gupta *et al.*, 2017] Jayesh K Gupta, Maxim Egorov, and Mykel Kochenderfer. Cooperative multi-agent control using deep reinforcement learning. In *Autonomous Agents and Multiagent Systems: AAMAS 2017 Workshops, Best Papers, São Paulo, Brazil, May 8-12, 2017, Revised Selected Papers 16*, pages 66–83. Springer, 2017.

[Hu and Zhang, 2022] Yizheng Hu and Zhihua Zhang. Sparse adversarial attack in multi-agent reinforcement learning. *arXiv preprint arXiv:2205.09362*, 2022.

[Huang *et al.*, 2017] Sandy Huang, Nicolas Papernot, Ian Goodfellow, Yan Duan, and Pieter Abbeel. Adversarial attacks on neural network policies. *arXiv preprint arXiv:1702.02284*, 2017.

[Inkawich *et al.*, 2020] Matthew Inkawich, Yiran Chen, and Hai Li. Snooping attacks on deep reinforcement learning. In *Proceedings of the 19th International Conference on Autonomous Agents and MultiAgent Systems*, pages 557–565, 2020.

[Kos and Song, 2017] Jernej Kos and Dawn Song. Delving into adversarial attacks on deep policies. *arXiv preprint arXiv:1705.06452*, 2017.

[Kurakin *et al.*, 2018] Alexey Kurakin, Ian J Goodfellow, and Samy Bengio. Adversarial examples in the physical world. In *Artificial intelligence safety and security*, pages 99–112. Chapman and Hall/CRC, 2018.

[Lin *et al.*, 2020] Jieyu Lin, Kristina Dzeparoska, Sai Qian Zhang, Alberto Leon-Garcia, and Nicolas Papernot. On the robustness of cooperative multi-agent reinforcement learning. In *2020 IEEE Security and Privacy Workshops (SPW)*, pages 62–68. IEEE, 2020.

[Liu and Lai, 2023] Guanlin Liu and Lifeng Lai. Efficient adversarial attacks on online multi-agent reinforcement learning. *Advances in Neural Information Processing Systems*, 36:24401–24433, 2023.

[Lv *et al.*, 2025] Yang Lv, Jinlong Lei, and Peng Yi. A local information aggregation-based multiagent reinforcement learning for robot swarm dynamic task allocation. *IEEE Transactions on Neural Networks and Learning Systems*, 36(6):10437–10449, 2025.

[Madry *et al.*, 2018] Aleksander Madry, Aleksandar Makelov, Ludwig Schmidt, Dimitris Tsipras, and Adrian Vladu. Towards deep learning models resistant to adversarial attacks. In *6th International Conference on Learning Representations, ICLR 2018, Vancouver, BC, Canada, April 30 - May 3, 2018, Conference Track Proceedings*. OpenReview.net, 2018.

[Moreno *et al.*, 2021] Pol Moreno, Edward Hughes, Kevin R. McKee, Bernardo Ávila Pires, and Théophane Weber. Neural recursive belief states in multi-agent reinforcement learning. *CoRR*, abs/2102.02274, 2021.

[Nisioti *et al.*, 2021] Eleni Nisioti, Daan Bloembergen, and Michael Kaisers. Robust multi-agent Q-learning in cooperative games with adversaries. In *Proceedings of the AAAI conference on artificial intelligence*, volume 2, 2021.

[Papernot *et al.*, 2016] Nicolas Papernot, Patrick McDaniel, and Ian Goodfellow. Transferability in machine learning: from phenomena to black-box attacks using adversarial samples. *arXiv preprint arXiv:1605.07277*, 2016.

[Papoudakis *et al.*, 2021] Georgios Papoudakis, Filippos Christianos, Lukas Schäfer, and Stefano V. Albrecht. Benchmarking multi-agent deep reinforcement learning algorithms in cooperative tasks. In Joaquin Vanschoren and Sai-Kit Yeung, editors, *Proceedings of the Neural Information Processing Systems Track on Datasets and Benchmarks 1, NeurIPS Datasets and Benchmarks 2021, December 2021, virtual*, 2021.

[Park *et al.*, 2024] Kidon Park, Hong-Gyu Jung, Tae-San Eom, and Seong-Whan Lee. Uncertainty-aware portfolio management with risk-sensitive multiagent network. *IEEE Trans. Neural Networks Learn. Syst.*, 35(1):362–375, 2024.

[Pham *et al.*, 2023] Nhan H Pham, Lam M Nguyen, Jie Chen, Hoang Thanh Lam, Subhro Das, and Tsui-Wei Weng. Attacking c-marl more effectively: A data driven approach. In *2023 IEEE International Conference on Data Mining (ICDM)*, pages 1271–1276. IEEE, 2023.

[Rakhsha *et al.*, 2020] Amin Rakhsha, Goran Radanovic, Rati Devidze, Xiaojin Zhu, and Adish Singla. Policy teaching via environment poisoning: Training-time adversarial attacks against reinforcement learning. In *Inter-*

*national Conference on Machine Learning*, pages 7974–7984. PMLR, 2020.

[Rakhsha *et al.*, 2021] Amin Rakhsha, Goran Radanovic, Rati Devidze, Xiaojin Zhu, and Adish Singla. Policy teaching in reinforcement learning via environment poisoning attacks. *Journal of Machine Learning Research*, 22(210):1–45, 2021.

[Rashid *et al.*, 2018] Tabish Rashid, Mikayel Samvelyan, Christian Schroeder, Gregory Farquhar, Jakob Foerster, and Shimon Whiteson. Qmix: Monotonic value function factorisation for deep multi-agent reinforcement learning. In *International Conference on Machine Learning*, pages 4295–4304. PMLR, 2018.

[Szegedy, 2013] C Szegedy. Intriguing properties of neural networks. *arXiv preprint arXiv:1312.6199*, 2013.

[Wu *et al.*, 2021] Xian Wu, Wenbo Guo, Hua Wei, and Xinyu Xing. Adversarial policy training against deep reinforcement learning. In *30th USENIX Security Symposium (USENIX Security 21)*, pages 1883–1900, 2021.

[Yu *et al.*, 2022] Chao Yu, Akash Velu, Eugene Vinitsky, Jiaxuan Gao, Yu Wang, Alexandre Bayen, and Yi Wu. The surprising effectiveness of ppo in cooperative multi-agent games. *Advances in Neural Information Processing Systems*, 35:24611–24624, 2022.

[Zhang *et al.*, 2020] Xuezhou Zhang, Yuzhe Ma, Adish Singla, and Xiaojin Zhu. Adaptive reward-poisoning attacks against reinforcement learning. In *International Conference on Machine Learning*, pages 11225–11234. PMLR, 2020.

[Zhang *et al.*, 2022] Xianjie Zhang, Yu Liu, Hangyu Mao, and Chao Yu. Common belief multi-agent reinforcement learning based on variational recurrent models. *Neurocomputing*, 513:341–350, 2022.

[Zhang *et al.*, 2024] Ying Zhang, Meng Yue, Jianhui Wang, and Shinjae Yoo. Multi-agent graph-attention deep reinforcement learning for post-contingency grid emergency voltage control. *IEEE Transactions on Neural Networks and Learning Systems*, 35(3):3340–3350, 2024.

[Zheng *et al.*, 2023] Haibin Zheng, Xiaohao Li, Jinyin Chen, Jianfeng Dong, Yan Zhang, and Changting Lin. One4all: Manipulate one agent to poison the cooperative multi-agent reinforcement learning. *Computers & Security*, 124:103005, 2023.

## A supplementary material

### A.1 Pseudo-codes

In Algorithm 1 and Algorithm 2 we provide the detailed pseudo-codes of align attack and PGD attack respectively.

---

#### Algorithm 1 Adversarial Attack to Induce Misalignment

---

- 1: **Input:** Data collection period  $\mathcal{T}^c$ , attack period  $\mathcal{T}^a$ , PGD parameters.
- 2: **Initialization:** Initialize  $f_\theta$  and the dataset  $\mathcal{D} = \emptyset$
- 3: **Phase One:** Data collection and model training
- 4: **for**  $t = 1$  to  $\mathcal{T}^c$  **do**
- 5:   Collect  $\{o_{1,t}, o_{2,t}, \dots, o_{n,t}\}$  and store it in  $\mathcal{D}$ .
- 6: **end for**
- 7: Train  $f_\theta$  using the collected dataset  $\mathcal{D}$
- 8: **Phase Two:** Adversarial attack on infected agents
- 9: **for**  $t = 1$  to  $\mathcal{T}^a$  **do**
- 10:   Compute the perturbation  $\delta$  using PGD (Algorithm 2)
- 11:   Inject the perturbations
- 12: **end for**

---



---

#### Algorithm 2 Projected Gradient Descent algorithm

---

- 1: **Input:** Trained neural network  $f$ , observations  $\mathbf{o}$ , attack budget  $\epsilon$ , step size  $\alpha$ , number of iteration  $K$ , loss function  $J$ , allowed observation values  $[o^{min}, o^{max}]$ .
- 2: **Initialization:** Perturbation  $\delta^{(0)} = 0$ , perturbed observation  $\tilde{\mathbf{o}}^{(0)} = \mathbf{o}$ .
- 3: **Output:** Perturbed observations:  $\tilde{\mathbf{o}}^{(0)} = \tilde{\mathbf{o}}^{(K)}$ .
- 4: **for**  $k = 1$  to  $K$  **do**
- 5:   Compute the gradient  $\nabla_{\tilde{\mathbf{o}}^{(k-1)}} J(\tilde{\mathbf{o}}^{(k-1)}; \theta)$
- 6:   Compute  $\delta^k$ :  

$$\delta^{(k)} = \alpha \times \text{sign}(\nabla_{\tilde{\mathbf{o}}^{(k-1)}} J(\tilde{\mathbf{o}}^{(k-1)}; \theta))$$
- 7:   Clip  $\delta^{(k)}$  to  $[-\epsilon, \epsilon]$
- 8:   Compute  $\tilde{\mathbf{o}}^{(k)}$   

$$\tilde{\mathbf{o}}^{(k)} = \tilde{\mathbf{o}}^{(k-1)} + \delta^{(k)}$$
- 9:   Clip  $\tilde{\mathbf{o}}^{(k)}$  to  $[o^{min}, o^{max}]$
- 10: **end for**

---

### A.2 Hadamard matrices

In our implementations, we generate Hadamard matrices using *Sylvester's construction*. It is important to note that Hadamard matrices exist only for specific dimensions: when  $d$  is a multiple of 4. To bypass the requirement that  $d$  must be a multiple of 4, we generate a full Hadamard matrix of size  $\tilde{d}$ , where  $\tilde{d}$  is the largest power of two such that  $\tilde{d} \leq d$ :

$$\tilde{d} = 2^{\lfloor \log_2 d \rfloor} \quad (12)$$

We then pad the remaining  $d - \tilde{d}$  columns with zeros. This padding affects neither orthogonality nor the budget constraint.

As an example when  $n = 3$  and  $d = 10$ , we generate the following matrix in Figure 12: the first  $\tilde{d} = 8$  columns correspond to the scaled partial Hadamard matrix, while the remaining  $d - \tilde{d} = 2$  columns are zero-padded to extend the dimensionality to  $d = 10$ .

$$\boldsymbol{\delta} = \begin{bmatrix} \epsilon & 0 & 0 \\ \epsilon & -\epsilon & \epsilon & -\epsilon & \epsilon & -\epsilon & \epsilon & -\epsilon & 0 & 0 \\ \epsilon & \epsilon & -\epsilon & -\epsilon & \epsilon & \epsilon & -\epsilon & -\epsilon & 0 & 0 \end{bmatrix} \quad \begin{array}{c} \hline \tilde{d} = 8 \\ \hline \end{array} \quad \begin{array}{c} \hline d = 10 \\ \hline \end{array}$$

Figure 12: Padded partial Hadamard matrix for  $n = 3, d = 10$ .

We can theoretically combine the Hadamard attack with the Align attack in two ways: (1) by using a scaled partial Hadamard matrix to initialize the adversarial perturbations in Algorithm 2, line 2; or (2) by encouraging the perturbations of the Align attack to be orthogonal by adding a penalty to Equation (6):

$$-\lambda \left\| \boldsymbol{\delta}^\top \boldsymbol{\delta} - \mathbf{I} \right\|_2^2. \quad (13)$$

We implemented these two approaches, but did not notice any substantial improvements. However, using the targeted version of the Align attack to select a subset of agents and injecting Hadamard perturbations proved very effective in our experiments.

### A.3 Experimental details

We provide full details on the used environments in table 5, 7, 6.

Environment	FO	PO	HC	$\dim(o_i)$	N
8x8-3p-2f	✓	✗	✗	15	3
8x8-3p-2f-coop	✓	✗	✓	15	3
1s-8x8-3p-2f	✗	✓	✗	15	3
2s-8x8-3p-2f	✗	✓	✗	15	3
2s-8x8-3p-2f-coop	✗	✓	✓	15	3
10x10-4p-2f	✓	✗	✗	18	4
10x10-4p-2f-coop	✓	✗	✓	18	4
1s-10x10-4p-2f	✓	✗	✗	18	4
2s-10x10-4p-2f	✓	✗	✗	18	4
2s-10x10-4p-2f-coop	✓	✗	✗	18	4

Table 5: Selected LBF environments: we select (FO) fully observable, (PO) partial observable, and (HC) highly cooperative tasks.

Environment	PO	SR	$\dim(o_i)$	N
tiny-4ag-sr-1	✓	$3 \times 3$	71	4
tiny-4ag-sr-2	✓	$5 \times 5$	183	4
tiny-4ag-sr-3	✓	$7 \times 7$	351	4
small-4ag-sr-1	✓	$3 \times 3$	71	4
small-4ag-sr-2	✓	$5 \times 5$	183	4
small-4ag-sr-3	✓	$7 \times 7$	351	4

Table 6: Selected RWARE environments we select sensory range (SR) of  $3 \times 3$ ,  $5 \times 5$  and  $7 \times 7$ .

Environment	PO	$\dim(o_i)$	N
27m_vs_30m	✓	285	27
10m_vs_11m	✓	105	10
MMM2	✓	176	10
protoss_5_vs_5	✓	92	5
terran_5_vs_5	✓	82	5
zerg_5_vs_5	✓	82	5

Table 7: Selected SMAC environments: all environments are partially observable (PO)

We trained QMIX and MAPPO agents using the hyperparameters specified in tables 8, 9, 10, and 11. We use the Epymarl library [Papoudakis *et al.*, 2021] for training. We only report hyperparameters that are different from the default values found in Epymarl configurations. For the RWARE benchmark, we only train MAPPO agents, as QMIX performs poorly at this task [Papoudakis *et al.*, 2021]. Once the training is complete, we freeze the policy weights.

We test with three different neural architectures:

- Feedforward neural network: It consists of three hidden layers with 1024 hidden units.
- Recurrent neural network: For LBF and SMAC, we use one recurrent layer with a hidden dimension of 1024. For RWARE, we use 2 consecutive layers.
- Encoder-only transformer: For RWARE and LBF, we use  $d_{\text{model}}=256$  and  $\dim_{\text{feedforward}}=2048$  with 16 heads. For SMAC, we use  $d_{\text{model}}=128$  and  $\dim_{\text{feedforward}}=1024$  with 8 heads.

We use a learning rate of 0.0001 and a batch size of 64. The feedforward and transformer networks are trained for 100 epochs, while the RNN network is trained for 300 epochs.

Table 8: QMIX Hyperparameters Used for SMAC and LBF benchmark

Hyperparameter	SMAC	LBF
Runner type	parallel	episode
Batch size per run	8	1
Network hidden dimension	128	64
Learning rate	0.001	0.0003
Standardise rewards	True	True
Use RNN	True	True
Epsilon anneal time	50000	200000
Target update interval	200	0.01
Training batch size	64	32
Maximum timesteps ( $t_{max}$ )	20,050,000	5050000

Table 9: MAPPO Hyperparameters for SMAC benchmark.

Environments	hdim <sup>1</sup>	lr	Stand <sup>2</sup>	ent	q_nstep	Buffer	Epochs
MMM2	64	0.0005	False	0.001	10	10	4
27m_vs_30m	64	0.0005	False	0.001	10	10	4
10m_vs_11m	128	0.001	True	0	5	8	10
SMACv2	128	0.0003	True	0.001	5	10	4
protoss_5_vs_5	64	0.0005	False	0.001	10	10	4
terran_5_vs_5	128	0.0003	True	0.001	5	10	4
zerg_5_vs_5	128	0.0003	True	0.001	5	10	4

<sup>1</sup>hdim: Network hidden dimension <sup>2</sup>Stand: Standardise rewards

Table 10: MAPPO Hyperparameters for LBF benchmark.

Environment	lr	hdim	Stand	RNN	q_nstep
8x8-3p-2f	0.0003	128	False	False	5
8x8-3p-2f-coop	0.0005	32	True	True	5
1s-8x8-3p-2f	0.0003	128	False	True	10
2s-8x8-3p-2f	0.0003	128	False	False	5
2s-8x8-3p-2f-coop	0.0005	128	True	True	5
10x10-4p-2f	0.0003	128	False	False	5
10x10-4p-2f-coop	0.0003	32	True	True	5
1s-10x10-4p-2f	0.0003	128	False	True	10
2s-10x10-4p-2f	0.0003	128	False	False	5
2s-10x10-4p-2f-coop	0.0005	128	True	False	5

#### A.4 Baselines:

We use the following baselines:

- *White box attack*: It is the most powerful attack; it assumes access to the agent policy. In our paper, the white-box perturbation corresponds to the perturbation that minimizes the probability (or the q-value for QMIX) of the optimal action:

$$\delta = \arg \min_{\delta} \pi(\mathbf{o} + \delta, a^*) \quad \text{s.t.} \quad \|\delta\|_{\infty} \leq \epsilon \quad (14)$$

- *Random attacks*: Most previous works used only uniform distributions  $\delta_i \sim \mathcal{U}(-\epsilon, \epsilon)$  and normal distributions  $\delta_i \sim \mathcal{N}(0, \epsilon^2)$ . In addition to these two distributions, we add a non-symmetric distribution and a temporally correlated noise: for the former, we use the exponential distribution  $\text{Exp}(\lambda)$ . The value of  $\lambda$  is chosen such that 99% of the sampled values satisfy the budget constraint:

$$\lambda = -\frac{\ln(0.01)}{\epsilon} \quad (15)$$

Table 11: MAPPO Hyperparameters for RWARE.

Environment	lr	Stand	RNN	q_nstep	$t_{max}$
tiny-4ag-sr-1	0.0005	False	False	10	25M
tiny-4ag-sr-2	0.0008	False	False	10	25M
tiny-4ag-sr-3	0.0008	False	False	10	25M
small-4ag-sr-1	0.0005	False	False	10	25M
small-4ag-sr-2	0.0008	False	True	10	25M
small-4ag-sr-3	0.0008	False	False	20	40M

As correlated noise, we use the Ornstein–Uhlenbeck (OU) process:

$$\delta_{t+1} = \delta_t + \theta(\mu - \delta_t)\Delta t + \sigma\sqrt{\Delta t}\mathcal{N}(0, 1) \quad (16)$$

In our experiments, we use:

$$\mu = \epsilon, \theta \approx \epsilon, \sigma \approx \frac{\epsilon}{10} \pm 0.001, \Delta t = 1$$

We test different values of attack budget  $\epsilon \in \{0.03, 0.05, 0.07, 0.09, 0.1, 0.15, 0.2\}$  for RWARE and SMAC and  $\epsilon \in \{0.1, 0.15, 0.2, 0.25, 0.5, 0.75\}$  for LBF.

## A.5 More results

We provide the following additional results

- Performance across different MARL algorithms: In the main paper, we reported attacks against MAPPO agents. In Figures 13 and 14 we compare the performance of our attack against MAPPO and QMIX. Both figures show that our approach works for both policy-based and value-based algorithms. On the LBF benchmark, the performance is nearly identical. For SMAC, however, the Align attack tends to be more impactful on QMIX agents at higher  $\epsilon$  values.
- Additional results for targeted align attacks: in Figures 15 16, 17 we show the performance of targeted align attack for all the environments.
- Additional result for the combination of align attack for selection and Hadamard attack for perturbation: Tables 12, 13, 14 present the effect of selecting agents using align a-network  $f_\theta$  and using Hadamard perturbations for all the 22 environments.
- Additional results on episode length: Table 15 shows the impact of Align attack on the episode lengths of all LBF tasks.

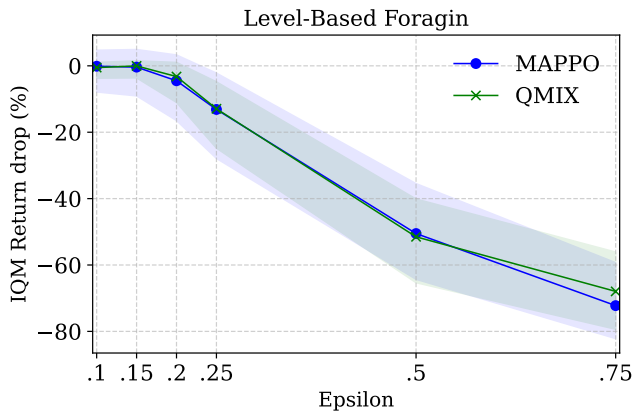


Figure 13: Performance across MARL algorithms on LBF.

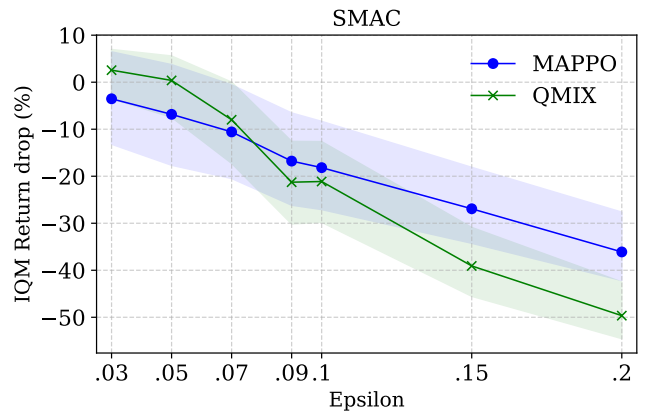


Figure 14: Performance across MARL algorithms on SMAC.

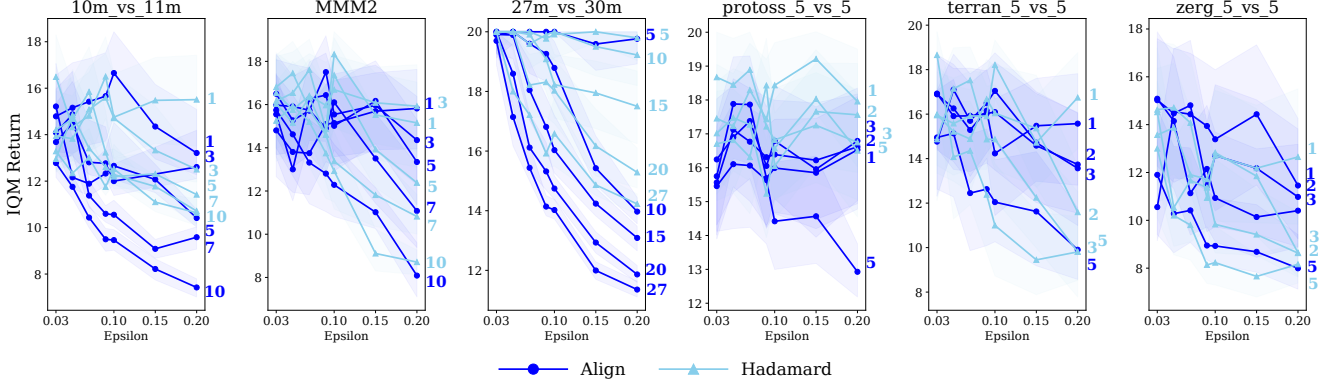


Figure 15: Performance of targeted align attacks on SMAC. For games with 10 agents, we report return curves when attacking 10, 7, 5, 3, and 1 agent(s). For games with 5 agents, we show the returns when targeting 5, 3, 2, 1 agent(s). For the 27m\_vs\_30m map, we report when having 27, 20, 15, 10, and 5 victims.

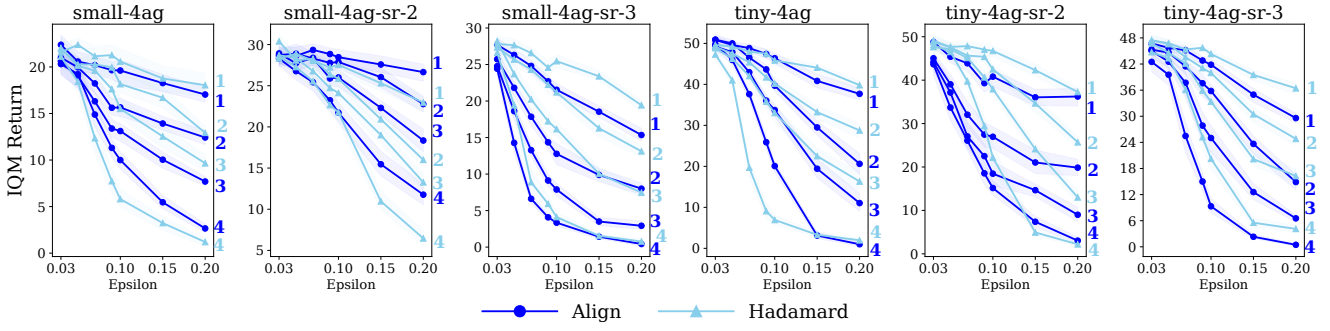


Figure 16: Performance of lighter attacks on RWARE. We report return curves when attacking 4, 3, 2, 3, and 1 agent(s).

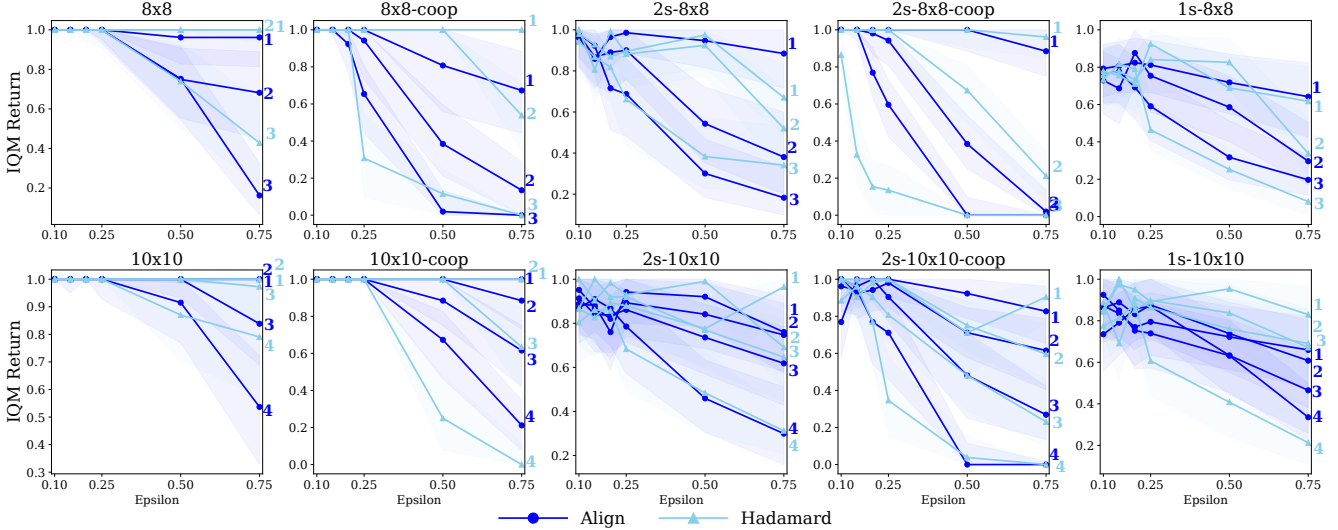


Figure 17: Performance of lighter attacks on LBF. For games with 3 agents, the first row, we report return curves when attacking 3, 2, and 1 agent(s). For tasks with 4 agents, the second row, we include the returns when targeting 4, 3, 2, 1 agent(s).

Task	$m$	$\epsilon = 0.15$	$\epsilon = 0.2$	$\epsilon = 0.25$
1s-10x10-4p-2f	2	-23.57	-4.99	-6.6
	3	2.32	-6.28	-7.48
2s-10x10-4p-2f	2	-10.02	-21	-8.57
	3	-10.49	-11.71	-15.26
2s-10x10-4p-2f-coop	2	-3.84	-15.36	-17.30
	3	-3.84	-13.46	-15.38
1s-8x8-3p-2f	1	-6.01	-0.96	-19.24
	2	-7.42	-0.79	-19.34
2s-8x8-3p-2f	1	-0.93	3.15	1.88
	2	3.75	-18.10	-11.17
2s-8x8-3p-2f-coop	1	0	-3.84	-3.84
	2	-32.69	-48.07	-57.69

Table 12: Targeted Hadamard attack on LBF

Task	$m$	$\epsilon = 0.05$	$\epsilon = 0.09$	$\epsilon = 0.15$
tiny-4ag-sr-1	1	0.22	-0.37	-4.50
	2	0.52	-1.12	-9.97
	3	-1.35	-2.1	-16.80
small-4ag	1	-9.80	-6.71	-2.35
	2	3.26	-11.61	-12.70
	3	-2.17	-14.51	-19.23

Table 13: Targeted Hadamard attack on RWARE

Task	$m$	$\epsilon = 0.05$	$\epsilon = 0.09$	$\epsilon = 0.15$
10m_vs_11m	3	-8.3	-10.17	-3.71
	7	-14.35	0.40	1.98
MMM2	3	3.26	0.73	-6.32
	7	-2.76	1.22	-7.10
protoss_5_vs_5	2	-4.40	-7.58	-4.10
	3	-10.10	-1.37	-4.88
terran_5_vs_5	2	4.05	-3.05	-19.48
	3	-12.35	-21.03	-5.15
zerg_5_vs_5	2	-22.28	-11.09	-3.77
	3	0.27	-12.86	-4.40

Table 14: Targeted Hadamard attack on SMAC

Tasks	0.1	0.15	0.2	0.25	0.5	0.75
1s-8x8	1.30	1.55	2.09	3.63	12.09	12.18
1s-10x10	-5.68	-9.66	2.26	7.94	16.64	22.88
2s-8x8-coop	9.59	43.55	138.52	152.49	170.86	170.86
2s-8x8	5.17	18.84	31.93	44.26	72.24	72.24
2s-10x10-coop	34.44	23.78	65.78	68.52	79.04	85.19
2s-10x10	12.45	-2.72	14.36	20.78	52.38	54.29
8x8-coop	10.59	29.67	103.86	188.56	226.80	226.80
8x8	5.94	21.06	51.93	75.93	193.21	285.80
10x10-coop	23.49	18.89	23.43	42.13	190.87	214.86
10x10	0.66	20.32	11.93	29.41	49.43	110.93

Table 15: Episode length increase (%) on LBF tasks